2023 45th Annual International Conference of the IEEE Engineering in Medicine & Biology Society (EMBC) | 979-8-3503-2447-1/23/$31.00 ©2023 IEEE | DOI: 10.1109/EMBC40787.2023.10340020

Non-invasive estimation of arterial blood pressure fluctuations using a peripheral photoplethysmograph inside the MRI scanner

Rémi Dagenais[1] and Georgios D. Mitsis[1], *Senior Member, IEEE*

***Abstract*— The blood-oxygen-level-dependent (BOLD) signal measured by functional magnetic resonance imaging (fMRI) is modulated by neural activity through the neurovascular coupling effect, as well as non-neural factors of physiological origin such as heart rate, respiration, and arterial blood pressure (ABP). While the former two effects have been previously characterized, the modulation of the BOLD signal by ABP fluctuations is still poorly understood. This is largely due to the difficulty of obtaining reliable ABP measurements in the MRI environment. Here, we propose a combined experimental and mathematical modeling framework to estimate ABP fluctuations inside the MRI scanner using photoplethysmography (PPG). Specifically, we used concurrent PPG and ABP measurements obtained outside the scanner to train the mathematical model and applied it to PPG measurements obtained inside the MRI scanner. Our results suggest good agreement between the model-predicted and experimentally measured ABP fluctuations and region specific correlations with the BOLD fluctuations.**

I. INTRODUCTION

The BOLD-fMRI signal is used to detect local neural activity indirectly through the neurovascular coupling effect [1]. This effect consists of a complex interplay between cerebral blood flow (CBF), cerebral blood volume (CBV), and cerebral metabolic rate of oxygen consumption (CMRO2) which parallels local glucose metabolism in the brain following neural activation [2]. As a result, local brain activity is observed as a BOLD increase due to an effective local increase in oxygenated haemoglobin in the venous compartments of activated brain regions.

This contrast mechanism is, however, also impacted by phenomena that modulate the interplay between CBF, CBV, and CMRO2 independently of neural activity. These physiological confounds include heart rate variability (HRV), respiratory flow (RF), and arterial blood pressure (ABP) fluctuations (see [3] for an exhaustive review on physiological confounds in resting-state fMRI). The effects of HRV and RF have been extensively studied previously using physiological recordings obtained concurrently with the BOLD-fMRI signal (see for example [4]). On the other hand, the relationship between the BOLD-fMRI signal and ABP fluctuations is less well studied, mostly due to the difficulty in reliably measuring this physiological signal inside the scanner.

*This work was supported by the Natural Sciences and Engineering Research Council of Canada (Discovery Grant 34362) and Fonds de recherche du Québec (Master's scholarship awarded to R. Dagenais)

[1]Rémi Dagenais is with the department of Bioengineering, McGill University, Montréal, QC H3A 0G4, Canada remi.dagenais@mail.mcgill.ca

[1]Georgios D. Mitsis is with the Department of Bioengineering, McGill University, Montréal, QC H3A 0G4, Canada georgios.mitsis@mcgill.ca

Previous attempts at characterising the impact of ABP fluctuations on the BOLD signal have used modified technologies to make them MRI compatible. [5], [6] used a modified version of the Finapres Nova system (Finapres Medical System, Enschede Netherlands), which was shielded from the MRI environment using a mu-metal box, to obtain continuous ABP measurements during phenylephrine injections and acute hypoxia and used these to study the involvement of the central autonomic network (CAN) in the human baroreflex and chemoreflex. [7] used an MRI compatible version of the CareTaker with an extended finger cuff (CareTaker Medical, Virginia USA) to obtain continuous ABP measurements during lower body negative pressure to study the involvement of the CAN in human cardiovascular regulation. [8], [9] also used the same MRI version of the CareTaker to study cerebral autoregulation using fMRI.

Implementing such modifications to measure ABP fluctuations during MRI may not be feasible in many cases, which has consequently limited the studies measuring ABP in the scanner. Here, we present a combined experimental and mathematical modeling methodology to accurately estimate ABP changes in the MRI environment using PPG measurements, which can be routinely recorded by most commercial scanners. The proposed method relies on performing a calibration session using an established ABP measurement method (e.g: Portapres, Finapres Medical System, Enschede Netherlands), identifying the most informative PPG waveform features and using these to predict ABP values. Since BOLD-fMRI is non-quantitative, we focus on predicting accurately the relative ABP fluctuations rather than the absolute values. Nonetheless, our method is based on PPG and as such could be generalized to other cases such as wearable devices.

II. METHODOLOGY

A. Experimental protocol

Calibration phase: To estimate ABP fluctuations in the MRI scanner, we acquired two five-minute calibration recordings outside the scanner. These included measurements using an MRI compatible PPG sensor and a non-MRI compatible continuous ABP monitor (Portapres) while the participant was at rest in a supine position. These recordings were used to train a mathematical model that is subsequently used to estimate ABP fluctuations using the PPG signal only during the scanning protocol. The calibration recordings can be acquired before and after the functional scan in the MRI control room.

Validation phase: To validate the accuracy of ABP estimation using calibration recordings, we acquired data during physiological manipulations that induced larger amplitude ABP fluctuations (controlled breathing and cold pressor test). Specifically, PPG and ABP were collected outside the scanner in ten healthy participants (20-27 years old, 5 females). The participants were asked to lie down in a supine position on a thin mattress for the duration of the acquisition. Each session consisted of 5 minute resting-state (eyes open), 6 minute controlled breathing (four repeated blocks of cued-breathing at 20 breaths/min for one minute followed by a 20 sec breath-hold), 12.5 minutes of a cold pressor stimulus (five application of a cold pressor on the left ankle for 60 seconds followed by the application of a room temperature cloth for 90 seconds), and a final 5 minute resting-state (eyes open). This protocol was also repeated in the MR scanner, where only PPG was measured.

B. Mathematical modeling

Mean arterial blood pressure (MAP) was extracted from the Portapres signal by detecting semi-automatically the systolic and diastolic points with PhysioPeaksFinder, a MATLAB graphical user interface (GUI) programmed in-house (https://github.com/DagenaisR/PhysioPeaksFinder). MAP is defined in (1), where SBP and DBP refer to systolic and diastolic blood pressure respectively.

$$MAP = \frac{(SBP + 2 \cdot DBP)}{3} \tag{1}$$

The MAP signal was re-sampled at 4Hz, band-passed with a fourth order Butterworth filter (0.008-0.15Hz), and then normalized such as to make it unit-variance.

The PPG signal was band-passed (0.5-10 Hz) using a fourth order Butterworth filter. The resulting signal was then separated into individual pulses to extract features semi-automatically. For each heartbeat, the diastolic point and the systolic and diastolic peaks were identified using PhysioPeaksFinder. The equivalent MAP point was also extracted in the PPG waveforms using (1). The amplitude and temporal position were extracted for each point (see Fig. 1) and the difference and first order interactions were computed (22 amplitude based features, and 7 temporal based features).

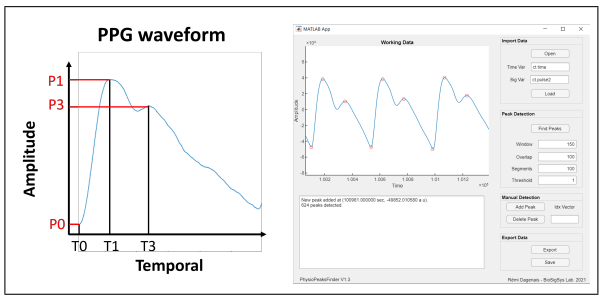

Fig. 1. Schematic of the semi-automatic extraction of the diastolic point (P0, T0), systolic peak (P1, T1), and the diastolic peak (P3, T3) performed using PhysioPeaksFinder (right). The midpoint between P1 and P0 was then obtained (Pm) as well as its location (Tm) between T0 and T1.

Following this, a decomposition of each pulse was performed using a temporal version of the Schrödinger equation as explained in [10]. Briefly, each pulse was decomposed into a sum of eigenvectors (10 in this case) by solving the eigenvalue problem shown in (2) with the MATLAB routine eig.

$$(-\mathbf{D}_2 - \chi \cdot \mathrm{diag}(\mathbf{y}))\mathbf{\Psi} = \boldsymbol{\lambda}\mathbf{\Psi} \tag{2}$$

Where $\mathbf{D}_2$ corresponds to the second-order differentiation matrix defined in [10] and presented in (3, 4):

- If $\mathbf{y}$ contains an even number of samples (N)

$$\mathbf{D}_2(k,j) = \frac{\Delta^2}{(\Delta t)^2} \begin{cases} \frac{-\pi^2}{3\Delta^2} - \frac{1}{12} \text{for k = j} \\ -(-1)^{k-j} \frac{1}{2\sin^2(\frac{(k-j)\Delta}{2})} \text{for k} \neq \text{j} \end{cases} \tag{3}$$

- If $\mathbf{y}$ contains an odd number of samples (N)

$$\mathbf{D}_2(k,j) = \frac{\Delta^2}{(\Delta t)^2} \begin{cases} \frac{-\pi^2}{3\Delta^2} - \frac{1}{12} \text{for k = j} \\ -(-1)^{k-j} \frac{\cot(\frac{(k-j)\Delta}{2})}{2\sin^2(\frac{(k-j)\Delta}{2})} \text{for k} \neq \text{j} \end{cases} \tag{4}$$

$$\text{with } \Delta = \frac{2\pi}{N}, \Delta t = \text{sampling rate} \tag{5}$$

where $k, j = 1...N$, χ is the scaling parameter which determines the number of eigenvectors used to decompose the pulse $\mathbf{y}$, $\mathbf{\Psi}$ is the wave equation, or mathematically, the eigenvector matrix, and $\boldsymbol{\lambda}$ are the eigenvalues. 19 features were extracted as in [11] from the eigenvalues and the pulse decomposition residuals.

Finally, the pulse low frequency signal ($\leq$0.5Hz) and the envelope (minimum and maximum of each pulse) were extracted (3 features). In total, 51 features were obtained from the PPG waveform and re-sampled at 4Hz. Outliers were detected and replaced with the nearest value and each feature was then band-passed with a fourth-order Butterworth filter (0.008-0.15Hz). All the features were normalized to a unit variance. An explicit description of each feature is presented in the MATLAB code provided in the GitHub repository (https://github.com/DagenaisR/EMBC23).

The subject-specific stacking model was trained using two recordings as calibrations. Once trained, the stacking model can predict MAP fluctuations from the PPG signal only. The modeling process is presented in Fig. 2.

Overall, the dimensionality of the highly co-linear features (amplitude and eigenvalue features) was first reduced by the base models using dynamic partial least square (dPLS) regression (PLS with time lagged features included in the regression matrix), and the resulting outputs were subsequently fed into an elastic net regressor along with the time lagged temporal and slow-fluctuations features.

III. Results

A. Model-predicted ABP fluctuations

The MAP fluctuations were estimated for the three conditions tested (resting-state, controlled breathing, and cold pressor test). The subject-specific stacked model was trained

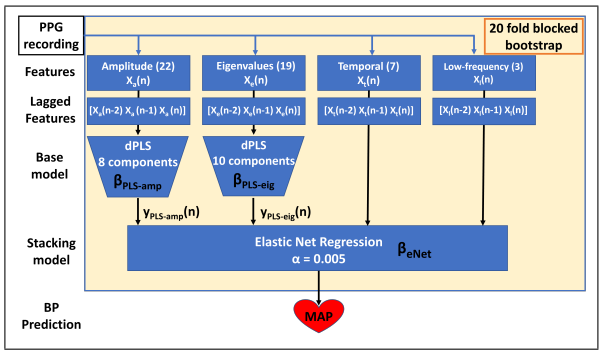

Fig. 2. Subject specific stacking model workflow used to predict the MAP fluctuations using the PPG signal only. In the first phase (**training**), the features and MAP from the calibration recordings (2 x 5 minutes) were randomly sampled in 20 blocks of 30 sec with replacement to train the model 20 times (20 fold blocked bootstrap). In the second phase (**prediction**), the validation data was used, and the final MAP prediction was obtained by averaging over the predictions given by the 20 trained models ($\beta_{PLS-amp}(i)$, $\beta_{PLS-eig}(i)$, $\beta_{eNet}(i)$, with i = 1 ... 20). The optimal number of time lagged features to include in the regression matrix, the PLS components for the base models, and the α parameter for the elastic net regression were determined using a search grid on a group level.

as per Fig. 2. Overall, eight out of the ten subjects could be processed to train the model. One subject (male) had to be rejected because it contained too many motion artifacts throughout the scans. Another subject (female) was rejected due to low signal-to-noise ratio (SNR), which made the peak detection impossible. The coefficient of determination (R^2) and Pearson's correlation (r) values between the model-predicted MAP fluctuations using the model and the true values (as measured with Portapres) are presented in Fig. 3.

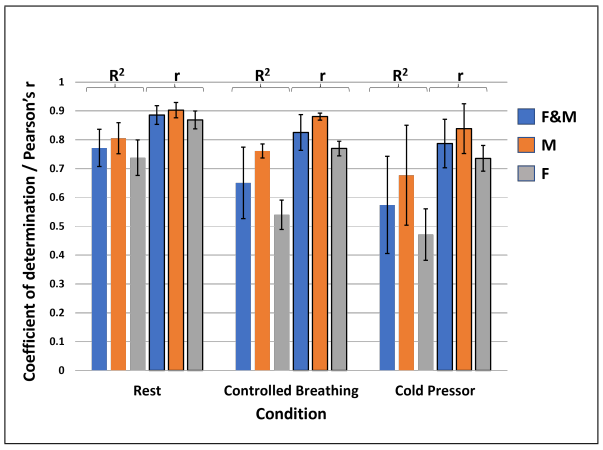

Fig. 3. Average R^2 and r between the predicted MAP fluctuations and the measured fluctuations (Portapres) for 8 subjects (F&M), and disaggregated between males (M) (N = 4) and females (F) (N = 4) as a function of the condition. The error bars denote standard deviation.

To provide a qualitative example of the resulting performance of the model, two subject specific predictions are presented in Fig. 4. These predictions can be considered as representative in the sense that their individual performance was the closest to the mean values presented in Fig. 3. The coherence function between the model-predicted and the true values is also presented to demonstrate the performance of the model as a function of frequency.

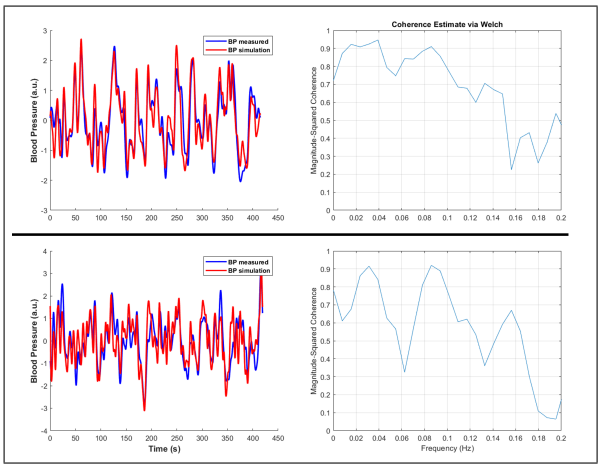

Fig. 4. Representative model-predicted MAP fluctuations for a male (top panel, R^2 = 0.76, r = 0.88) and a female (bottom panel, R^2 = 0.51, r = 0.76) subject during the controlled breathing task. The coherence function between the measured and model-predicted MAP fluctuations is presented on the right.

B. Correlation between ABP fluctuations and BOLD-fMRI

Results are presented for a specific subject (male) during the controlled breathing task, where the global BOLD-fMRI signal (GS) and the model-predicted MAP fluctuations were averaged over the four repeated blocks of breath-hold/cued breathing (Fig. 5). The controlled breathing task modulated the MAP fluctuations and the GS similarly over the four repeats (R^2 = 0.61).

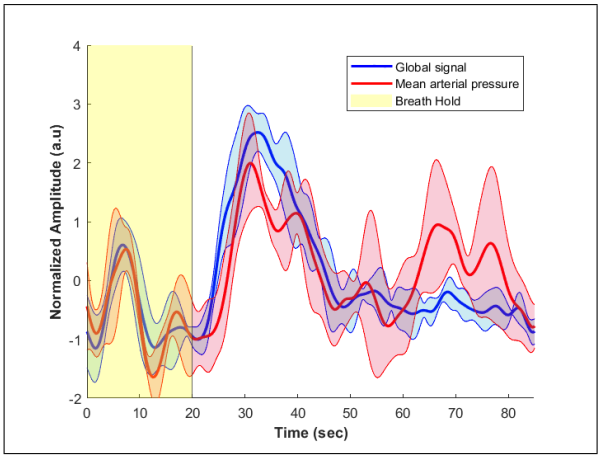

Fig. 5. Representative GS and model-predicted MAP fluctuations averaged over four repeated breath-holds (20 sec), followed by cued-breathing (20 breaths/min). The shaded area presents the standard deviation over the four repetitions.

We also investigated the correlation between the ABP fluctuations and the BOLD-fMRI signal on a voxel-wise level averaged over five participants (2 females) for the three examined conditions. Briefly, the MAP fluctuations were convolved with an impulse response function modeled as a double gamma function to predict the GS on a subject level (see [4] for a detailed analysis with HRV and RF). The resulting subject-specific ABP response was correlated voxel-wise with the local BOLD signal. The resulting cor-

relation maps were then averaged for the five participant for the three different conditions tested (Fig. 6).

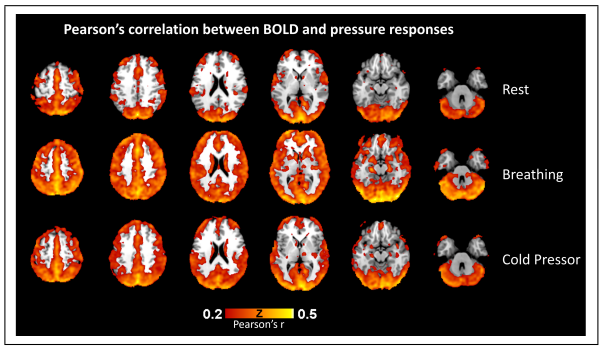

Fig. 6. Group level (N = 5) voxel-wise Pearson's correlation values (r) between the ABP responses and the local BOLD signal for all three conditions.

IV. Discussion

We describe a novel methodology to estimate ABP fluctuations in the MRI environment. The pre-scan and post-scan calibrations are used to train the model. Our results show that the proposed methodology is able to accurately estimate ABP fluctuations during the resting-state and physiological manipulations, and that the ABP estimates in the MR scanner were correlated to BOLD signal fluctuations during all experimental conditions.

We did not compare the performance of our methodology with the existing literature on ABP estimation using PPG mainly because these studies have been mostly conducted on the MIMIC II database, which does not represent a healthy population [12]. Moreover, the majority of these studies did not report R^2 and r statistics, but rather the mean absolute error, standard deviation, and cumulative percentage error. These statistical measures are recommended by the BHS and AAMI standards for testing the reliability of ABP monitors [13], [14]. Considering that the main interest of the present work was BOLD-fMRI, which is non-quantitative, we were mostly interested in the relative ABP fluctuations, which are better described by R^2 and r.

The principal limitation of this study, but not specific to it, is that the prediction performance scales with the SNR of the PPG measurements. In general, participants with smaller hands and poor peripheral perfusion typically yield a lower SNR. In our small sample size, we found that this was more often the case with female participants, especially after lying in a supine position for a few minutes. This resulted in an inferior performance for this group for all conditions (Fig. 3). Similarly, the SNR generally decreased during the controlled breathing and cold pressor stimulus tasks, which also resulted in inferior performance when compared to resting-state prediction.

The sex-dependent performance may partly explains the discrepancy between female and male participants in the aforementioned studies ([5], [6], [8], [9]) where 83% of all participants were male. This highlights the need for looking at sex differences in the context of ABP estimation and for studies that better represent the whole population. This is critical to prevent a potentially negative over generalization of the research findings.

Based on our observations, the model-predicted ABP fluctuations could be improved by optimizing the experimental protocol. While more informative features or a better model could improve the performance, we found that the proposed model yielded reliable results when clean waveforms were acquired. As such, future improvements to this work will focus on acquiring more data while minimizing the noise through the experimental protocol.

Finally, the GS and model-predicted MAP fluctuations obtained during the controlled breathing task (Fig. 5) suggest a considerable degree of correlation between the two signals. The group level correlation maps shown in Fig. 6 highlight regions that are highly susceptible to physiological confounds [4] during all conditions and show similar correlation patterns as [8], suggesting a potential application to our methodology for BOLD-fMRI denoising and studies of the autonomic brain centers.

Acknowledgment

We would like to acknowledge Mary Miedema and Emad Askarinejad for their help in the data collection process.

References

[1] N. K. Logothetis and B. A. Wandell, "Interpreting the BOLD signal," Annu. Rev. Physiol., vol. 66, pp. 735-769, 2004.
[2] P. T. Fox and M. E. Raichle, "Focal physiological uncoupling of cerebral blood flow and oxidative metabolism during somatosensory stimulation in human subjects," Proceedings of the National Academy of Sciences, vol. 83, no. 4, pp. 1140-1144, 1986.
[3] K. Murphy, R. M. Birn, and P. A. Bandettini, "Resting-state fMRI confounds and cleanup," Neuroimage, vol. 80, pp. 349-359, 2013.
[4] M. Kassinopoulos and G. D. Mitsis, "Identification of physiological response functions to correct for fluctuations in resting-state fMRI related to heart rate and respiration," Neuroimage, vol. 202, p. 116150, 2019.
[5] D. A. Gerlach et al., "Novel approach to elucidate human baroreflex regulation at the brainstem level: pharmacological testing during fMRI," Frontiers in neuroscience, vol. 13, p. 193, 2019.
[6] D. A. Gerlach et al., "Medullary and hypothalamic functional magnetic imaging during acute hypoxia in tracing human peripheral chemoreflex responses," Hypertension, vol. 77, no. 4, pp. 1372-1382, 2021.
[7] J. Manuel et al., "Deciphering the neural signature of human cardiovascular regulation," Elife, vol. 9, p. e55316, 2020.
[8] J. R. Whittaker, I. D. Driver, M. Venzi, M. G. Bright, and K. Murphy, "Cerebral autoregulation evidenced by synchronized low frequency oscillations in blood pressure and resting-state fMRI," Frontiers in neuroscience, vol. 13, p. 433, 2019.
[9] J. R. Whittaker, J. J. Steventon, M. Venzi, and K. Murphy, "The spatiotemporal dynamics of cerebral autoregulation in functional magnetic resonance imaging," Frontiers in Neuroscience, vol. 16, 2022.
[10] T.-M. Laleg-Kirati, E. Crépeau, and M. Sorine, "Semi-classical signal analysis," Mathematics of Control, signals, and Systems, vol. 25, pp. 37-61, 2013.
[11] P. Li and T.-M. Laleg-Kirati, "Central blood pressure estimation from distal ppg measurement using semiclassical signal analysis features," IEEE Access, vol. 9, pp. 44963-44973, 2021.
[12] M. Saeed et al., "Multiparameter Intelligent Monitoring in Intensive Care II (MIMIC-II): a public-access intensive care unit database," Critical care medicine, vol. 39, no. 5, p. 952, 2011.
[13] E. O'brien, B. Waeber, G. Parati, J. Staessen, and M. G. Myers, "Blood pressure measuring devices: recommendations of the European Society of Hypertension," Bmj, vol. 322, no. 7285, pp. 531-536, 2001.
[14] A. f. t. A. o. M. Instrumentation, "American national standards for electronic or automated sphygmomanometers," ANSI/AAMI SP 10-1987, 1987.